Langmuir

ARTICLE

pubs.acs.org/Langmuir

Correlating Interface Heterostructure, Charge Recombination, and Device Efficiency of Poly(3-hexyl thiophene)/TiO_2 Nanorod Solar Cell

Tsung-Wei Zeng,[†] Chun-Chih Ho,[†] Yu-Chieh Tu,[†] Guan-Yao Tu,[‡] Lee-Yih Wang,[‡] and Wei-Fang Su*[,†,‡]

[†]Department of Materials Science and Engineering and [‡]Institute of Polymer Science and Engineering, National Taiwan University, Taipei, Taiwan

Supporting Information

ABSTRACT: The charge recombination rate in poly(3-hexyl thiophene)/TiO_2 nanorod solar cells is demonstrated to correlate to the morphology of the bulk heterojunction (BHJ) and the interfacial properties between poly(3-hexyl thiophene) (P3HT) and TiO_2. The recombination resistance is obtained in P3HT/TiO_2 nanorod devices by impedance spectroscopy. Surface morphology and phase separation of the bulk heterojunction are characterized by atomic force microscopy (AFM). The surface charge of bulk heterojunction is investigated by Kelvin probe force microscopy (KPFM). Lower charge recombination rate and lifetime have been observed for the charge carriers in appropriate heterostructures of hybrid P3HT/TiO_2 nanorod processed via high boiling point solvent and made of high molecular weight P3HT. Additionally, through surface modification on TiO_2 nan,orod, decreased recombination rate and longer charge carrier lifetime are obtained owing to creation of a barrier between the donor phases (P3HT) and the acceptor phases (TiO_2). The effect of the film morphology of hybrid and interfacial properties on charge carrier recombination finally leads to different outcome of photovoltaic $I-V$ characteristics. The BHJ fabricated from dye-modified TiO_2 blended with P3HT exhibits 2.6 times increase in power conversion efficiency due to the decrease of recombination rate by almost 2 orders of magnitude as compared with the BHJ made with unmodified TiO_2. In addition, the interface heterostructure, charge lifetime, and device efficiency of P3HT/TiO_2 nanorod solar cells are correlated.

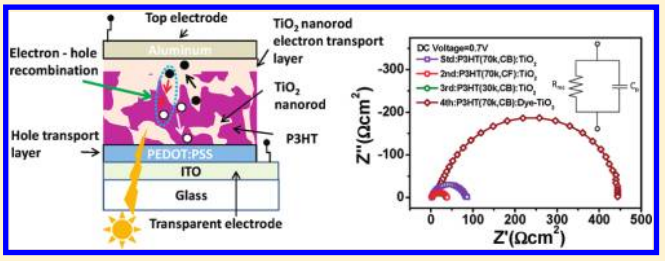

INTRODUCTION

Bulk heterojunction (BHJ) structures, constructed from a mixture of electron-donating and electron-accepting materials, have attracted great interest for the development of large-area and inexpensive polymer photovoltaic cells.[1,2] Several groups have reported that efficiency of bulk heterojunction polymer solar cells of over 7% is attained.[3,4] Formation of adequate charge carriers' transporting paths is necessary for the fabrication of efficient BHJ solar cells.[5−8] Bicontinuous network is needed for charge carriers' transporting paths, so that the photoinduced electron and hole can be extracted from the light absorber layer to the electrodes without recombination. Among the photo-to-electric conversion procedures in a solar cell, the charge carriers' recombination plays a major role in the solar cell device $I-V$ curve and on the efficiency. Therefore, characterization of the recombination resistance at the interface can provide essential information on device characteristics. The impedance characteristic at the interface can be evaluated by impedance spectroscopy (IS), which has been applied in the study of recombination in quantum dot-sensitized solar cells[9−12] and polymer BHJ solar cells.[13−17] IS is also a well-known technique for the study of electrochemical systems and has been extensively employed in the study of dye-sensitized solar cell characteristics[18,19] and polymer light-emitting diodes.[20]

One of the most important factors that can influence charge recombination is the heterostructure and interface. Recombination mostly takes place at the interface between respective electron and hole charge-transporting phases. Inadequate structures of donor/acceptor (D/A) separated phases lead to increased recombination at interfaces. For instance, as the continuity of the charge transporting phases is decreased, a fraction of the carriers will be trapped at dead ends of charge-transporting network since they cannot be transported to another transporting phase. These charges will eventually recombine with surrounded opposite charges.[7] In addition, larger interfacial area may increase bimolecular recombination sites.

Blending of conjugated polymers with promising acceptor material, inorganic nanocrystals, has been investigated for potential high-efficiency solar cells[7,8,21−24] and light-emitting diodes.[25] The continuity and domain size of donor and acceptor are determined by the extent of phase separation, which could be controlled through the fabrication parameters of hybrid materials. For the light absorber poly(3-hexyl thiophene) (P3HT) in combination with an acceptor for BHJ solar cell, the size and degree of nanodomain and fibril structure of P3HT can be

Received: September 8, 2011
Revised: October 29, 2011
Published: November 03, 2011

controlled by fabrication factors including the molecular weight of P3HT and the solvent evaporation speed for growth of the film.[26−29] In this study, varied charge carrier recombination processes are observed in P3HT/TiO_2 nanorod devices with different bulk heterostructures. We correlate the heterostructure and interface of the devices with their charge recombination behavior and device efficiency. Surface morphology and phase separation are resolved by atomic force microscopy (AFM). Kelvin probe force microscopy (KPFM) is applied to resolve the degree and dimension of phase separation and surface charge accumulation in polymer bulk heterojunctions.[30−34]

Other factors can also influence the charge carrier recombination in the solar cells. Due to the recombination occurs almost exclusively at the heterojunction, the interfacial recombination process is believed can be changed through modifications at the interfaces.[18] Anchoring a layer of molecule can shield the recombination process by blocking the holes to recombination centers on interfaces.[21,35−37]

In this research, the TiO_2 nanorods are incorporated into the P3HT in solution to fabricate the active layer P3HT/TiO_2 of polymer solar cell in a single step spin coating process at room temperature. The TiO_2 nanorods are used as only acceptor without [6,6]-phenyl-C61-butyric acid methyl ester (PCBM). The TiO_2 nanorods are prepared by sol−gel method at a low temperature of 98 °C. These TiO_2 nanorods can provide one-dimensional straight paths for efficient electron transporting in the bulk heterojunction. One-dimensional TiO_2 nanostructure is of great interest for serving as a component in polymer solar cells. By infiltrating P3HT into dye-modified TiO_2 nanotube array at 150 °C, the solar cell's efficiency of 3.8% has been attained. The TiO_2 nanotube array was prepared by electrochemical etching of Ti film and then heat-treated at 450 °C.[38] It has been reported that, by incorporating TiO_2 nanowires with P3HT/PCBM, the solar cell's efficiency of 1.27% has been achieved. The TiO_2 nanowires were obtained by electron spinning and were calcined at 450 °C.[39]

The interface of P3HT/TiO_2 in this study is modified by capping a benzothiadiazole-based dye molecule (W-4) on the TiO_2 surface. By use of the capped dye molecule on TiO_2, the recombination resistance is increased as shown by the study of IS that results in an increased photovoltaic device performance by 2.6 times.

MATERIALS AND METHODS

The TiO_2 nanorod (~3 nm × 20 nm) was synthesized according to the literature.[40,41] The as-synthesized TiO_2 nanorod was capped by oleic acid. The surface of the TiO_2 nanorod was modified by pyridine treatment following the approach in the literature[21] to remove the original surface ligand of oleic acid on TiO_2 surface. A dye molecule, 2-cyano-3-(5-(7-(thiophen-2-yl)-2,1,3-benzothiadiazol-4-yl)thiophen-2-yl) acrylic acid (W-4), has been anchored on the surface of pyridine treated TiO_2 to modify the surface properties through the process used in prior study.[21] The different molecular weight of P3HT with PDI < 1.5 and regioregularity (rr) > 95% was synthesized according to literature.[42]

To synthesize W-4, 5-[7-(thiophen-2-yl)-2,1,3-benzothiadiazol-4-yl]thiophene-2- carbaldehyde (0.9983 g, 3.04 mmol), cyanoacetic acid (0.19 g, 2.2 mmol), and ammonium acetate (28 mg, 0.4 mmol) were dissolved in acetic acid (50 mL) in a round flask. The solution was heated to reflux for 8 h andthen cooled down to ambient temperature. Deionized water (100 mL) was poured into the mixture, leading to precipitation. The crude product was washed with water, methanol, and ethyl ether several times and dried over 50 °C under vacuum for several hours. A red solid was obtained (W-4). ^{1}H NMR (ppm, DMSO-d_6): 7.28 (dd, 1H), 7.81 (d, 1H), 8.08 (d, 1H), 8.14 (d, 1H), 8.21 (d, 1H), 8.26 (d, 1H), 8.29 (d, 1H), 8.52 (s, 1H). ^{13}C NMR (DMSO-d_6): 98.83, 116.45, 123.30, 125.46, 126.95, 127.81, 127.83, 128.19, 128.21, 129.23, 136.68, 138.05, 139.84, 146.41, 147.24, 151.47, 151.52, 163.52. MS (m/z): 394.9. Detailed synthesis and characterization of W-4 are described in the Supporting Information.

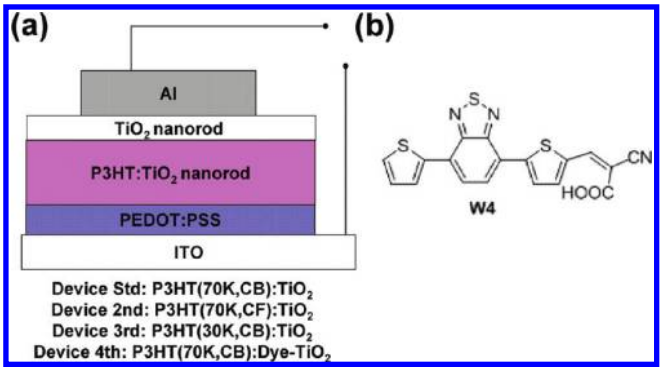

Figure 1. (a) Schematic diagram of P3HT/TiO_2 nanorod device structure. (b) Chemical structure of the interfacial modifier dye W-4.

Films of blends of P3HT in combination with pyridine-treated or dye-modified TiO_2 nanorods (P3HT/TiO_2) were prepared by spin-coating on indium tin oxide (ITO)/[poly(3,4-ethylenedioxythiophene)/poly(styrenesulfonate)] (PEDOT/PSS) substrates following the approach in the literature.[41] The hybrid P3HT/TiO_2 nanorods (47:53 wt %) films were first prepared from coating solutions of TiO_2 nanorods in a mixed solvent that contains pyridine, chloroform, and dichloromethane (1:3:2 by volume ratio) and P3HT in chlorobenzene (CB) or chloroform (CF), followed by coating a pure TiO_2 nanorod layer (~20 nm) from its pyridine solution. The 100 nm Al electrode was vacuum-deposited on top of the device.

The film morphology was observed by atomic force microscopy (AFM) (Digital Instruments Nanoscope III). The surface potential images were recorded by KPFM (Veeco Instruments multimode AFM with an extender electronics module) operating in the lift mode (typical lift height 20 nm) by silicon cantilevers with a PtIr surface coating in the dark or under white light illumination source (5 mW/cm^2). Impedance spectroscopy (IS) has been carried out under dark by varying applied direct current (dc) voltage. The 50 mV alternating current (ac) perturbation was used in impedance measurements with a frequency range from 3 MHz to 10 Hz. The current−voltage characterization ($I-V$) (Keithley 2400 source meter) was performed with a calibrated solar simulator under air mass (AM) 1.5G condition (Oriel Instruments) with irradiation intensity of 100 mW/cm^2. Once the power from the simulator was determined, a 400 nm cutoff filter was used to remove the UV light.

RESULTS AND DISCUSSION

We have investigated the effect of recombination rate on the performance of P3HT/TiO_2 nanorod hybrid solar cell. Figure 1a illustrates the schematic diagram of the BHJ devices with a structure of ITO/PEDOT/PSS/P3HT/TiO_2 nanorod/TiO_2

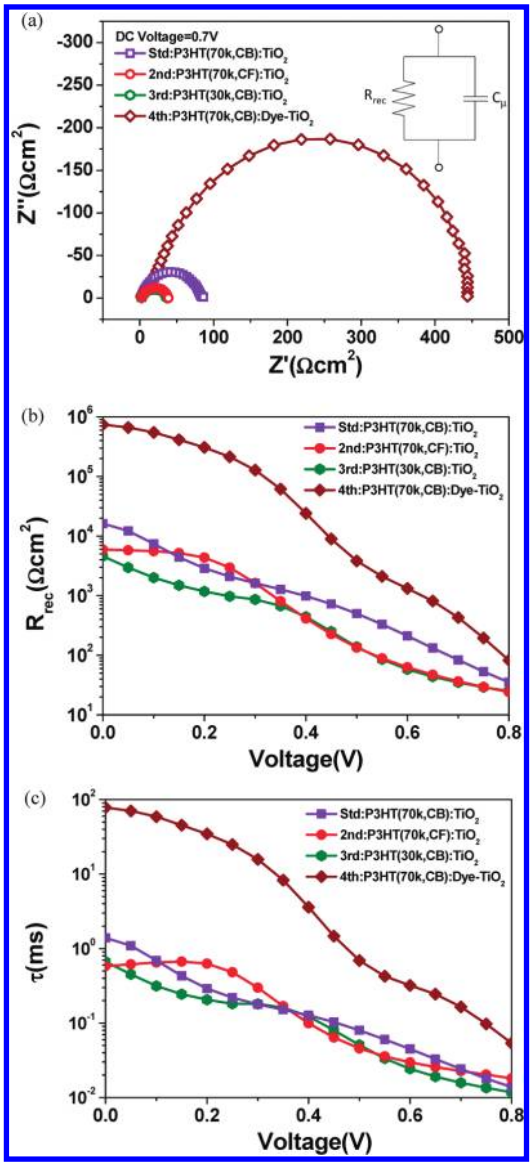

Figure 2. (a) Comparison of the Nyquist plot of the four types of devices under certain dc voltage (0.7 V). (Inset) ac equivalent circuit with recombination resistance (R_{rec}) and chemical capacitance (C_μ). (b) Comparison of the extracted recombination resistance (R_{rec}) as a function of applied dc voltage for the four devices. (c) Comparison of electron lifetime ($\tau = R_{rec}C_\mu$) as a function of applied dc voltage for the four devices.

nanorod/Al made from four kinds of bulk heterojunctions. For a standard device structure, the BHJ is made from 70K molecular weight of P3HT and TiO_2 nanorod in chlorobenzene (CB) solvent. In order to study the effect of BHJ type on recombination and cell efficiency, the change is only made in the BHJ while the rest of the parameters are kept identical to the standard structure. The BHJ of the second device was fabricated from a lower boiling point solvent of chloroform (CF) instead of CB. The BHJ of the third device was fabricated from a lower molecular weight of P3HT (30K). The changes of charge recombination and device efficiency are believed to be due to the altered P3HT crystalline size and phase separation in the absorber of the hybrid. The BHJ of the forth device is made from the blend of P3HT with dye-modified TiO_2 nanorod, which allows us to study the influence of the interfacial properties of P3HT/TiO_2 nanorod on recombination within the device. W-4 dye is used in device 4; its chemical structure is shown in Figure 1b. Detailed synthesis and characterization of W-4 are described in the Supporting Information.

We have studied the influence of fabrication parameters on the recombination of charge carriers in the devices. To obtain the recombination resistance and lifetime of charge carriers, impedance spectroscopy (IS) has been applied for the investigation. Figure 2a presents the complex plane plot of the obtained impedance for different devices at certain dc applied voltage. The impedance (Z) is separated into real (Z') and imaginary (Z'') parts as $Z = Z' + iZ''$. A predominant RC (resistor−capacitor) semicircle arc is observed in the complex plane plot, and a much smaller RC arc is found at high frequency. Typically, the high-frequency semicircle is related to the transport and series resistance, which is relatively small and can hardly be observed in the left corner of the plot. From the literature, we know that the low-frequency arc is mainly attributed to recombination in the active layer of conjugated polymer-based photovoltaic cells as well as the capacitance, resistance, and lifetime values as a function of applied bias.[14] To quantify the recombination rate in the devices, the predominant arc of impedance spectra was fitted into a frequently used equivalent circuit model,[9] where a recombination resistance (R_{rec}) is in parallel with a chemical capacitance (C_μ), as shown in the inset of Figure 2a.Toward the right side of the plots, we can see the size of the semicircle arc is highly dependent on the heterostructure in the devices. The impedance of the device was decreased from the standard device (purple curve) when the device was fabricated from either lower boiling point chloroform (red curve) or lower molecular weight P3HT (green curve). The results indicate undesired charge recombination interfaces and morphology were formed. The impedance of the device was greatly increased when the device was fabricated with dye-modified TiO_2 (brown curve), which reveals the dye functioning as an effective barrier to reduce the charge recombination.

An important factor in explaining the solar cell characteristics is the charge recombination. The recombination resistance was obtained from the fitting of IS spectra of these devices under various DC applied voltages from 0 to 0.8 V. The result shows an exponential decrease going downward with increasing dc voltage (Figure 2b). As compared with the standard device (purple curve), by changing the solvent from high boiling point CB to low boiling point CF (red curve) and lowering the molecular weight of P3HT (green curve), R_{rec} is decreased. Lowered recombination resistance is attributed to variation of P3HT/TiO_2 morphology. Increased possibility of bimolecular recombination rate is believed to be due to decreased connectivity of charge transporting paths or changed interface structures within devices processed with lower boiling point CF or composed of lower molecular weight P3HT. For the standard device, adequate heterostructures of charge transport channels create suitable interfaces and reduce the dead ends of interconnecting network. On the contrary, R_{rec} is increased by almost 2 orders of magnitude (brown curve) when the dye-modified TiO_2 was used in the device. The interfacial layer of the dye reduces the recombination of charge carriers due to the creation of a recombination barrier between the donor phases (P3HT) and the acceptor phases (TiO_2).

In polymer solar cells, the electron and hole have to be present in each separate phase to be transported to the opposite electrode. Therefore, interfacial recombination processes are significant at the boundary of these two phases. The interfacial

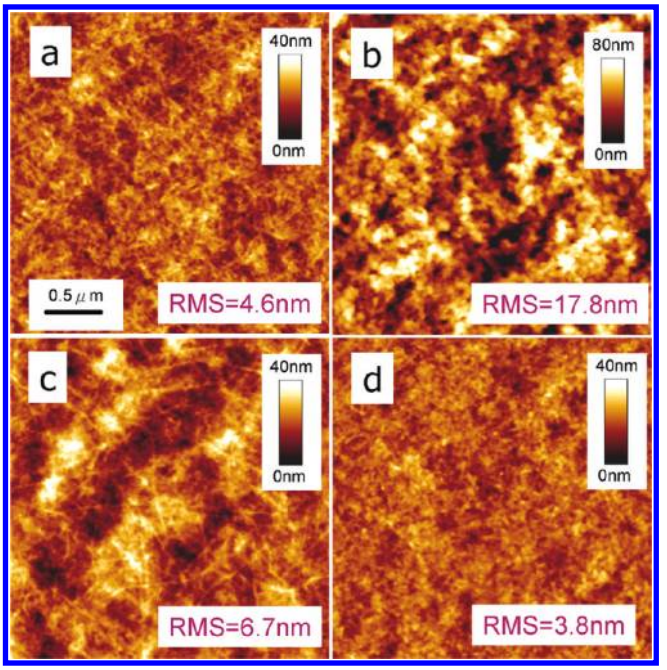

Figure 3. AFM surface morphological images for the active layer of the four devices: (a) standard device, P3HT(70K, CB)/TiO_2; (b) second device, P3HT(70K, CF)/TiO_2; (c) third device, P3HT(30K, CB)/TiO_2; (d) fourth device, P3HT(70K, CB)/dye-TiO_2.

recombination process can be inhibited through interfacial modification by anchoring a layer of molecules.[18] This layer may shield the recombination processes by blocking access of holes in P3HT to electrons in TiO_2. A second effect on polymer solar cell recombination rate by the adsorbed dye molecule is the introduction of a molecular dipole.[12,43] A layer of interfacial dipoles due to the existence of the dye with carboxylic acid group is formed between TiO_2 and the polymer. Due to interactions at the interfaces, the interfacial dipole layer alters the electrostatic potential energy across the interface. This is dependent on the concentration of the adsorbed dye molecule. As a result, the conduction-band level of TiO_2 and highest occupied molecular orbital (HOMO) of P3HT may be shifted and leads to changed driving force of charge recombination between TiO_2 and P3HT.

The electron lifetime τ for first-order recombination, defined as $\tau = R_{rec}C_{\mu}$,[9] can be derived from the results of the IS study. The result is shown in Figure 2c. Similarly, the electron lifetime is also highly dependent on the morphology and dye molecule interfacial modification of the bulk heterostructure. As compared with the standard device (purple curve), by changing the solvent from high boiling point CB to low boiling point CF (red curve) and lowering the molecular weight of P3HT (green curve), the electron lifetime is decreased. In addition, the electron lifetime is greatly increased (brown curve) when the dye-modified TiO_2 is used in the device.

The variation of charge recombination of the devices is affected by structure and interconnectivity of the hybrid material of P3HT and TiO_2. AFM measurement is applied to resolve the nanostructure or nanocrystallinity of P3HT and the film roughness (root-mean-square, rms). The hybrid film of standard device (Figure 3a) shows uniform surface morphology with nanofibril structure as well as an interconnected network due to the slow solvent evaporation speed of CB. The low boiling point solvent CF leads to rapid evaporation and reduces the crystallization time

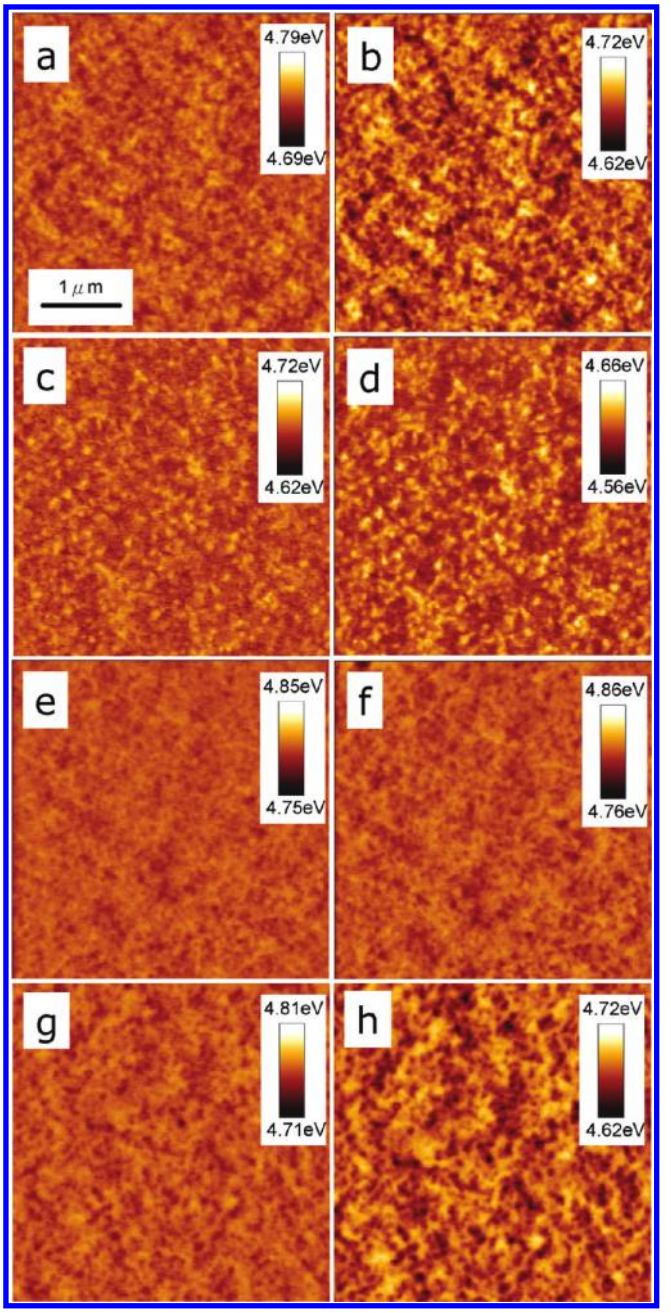

Figure 4. KPFM surface potential images in the dark and under illumination for the active layer of the four devices. Standard device, P3HT (70K, CB)/TiO_2 (a) in dark and (b) under illumination. Second device, P3HT (70K, CF)/TiO_2 (c) in dark and (d) under illumination. Third device, P3HT (30K, CB)/TiO_2 (e) in dark and (f) under illumination. Fourth device, P3HT (70K, CB)/dye-TiO_2 (g) in dark and (h) under illumination.

of P3HT during the spin-coating process. The coarse film prepared from CF solution appears less crystalline and has a granular topography (Figure 3b). When P3HT with lower molecular weight (30K) is used, the surface roughness is increased and surface uniformity is decreased (Figure 3c) as compared to the standard sample. For the sample made of dye-modified TiO_2 nanorods, the film surface is smooth and dense (Figure 3d), indicating the surface modification improves the mixing between P3HT and TiO_2.

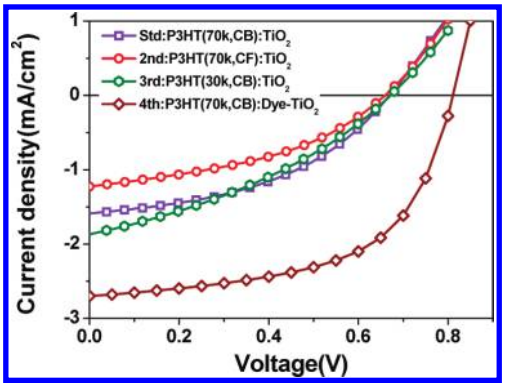

Figure 5. *I*−*V* curves of the four devices under AM 1.5G illumination.

Figure 4 displays the surface potential images of the blends in the dark and under illumination. The contrast is explained due to the differences in the alignment of the energy levels of the domains of respective donor (P3HT) -rich and acceptor (TiO_2) -rich materials with the Fermi level of the bottom electrode.[33] Figure 4a shows the TiO_2 nanorod-rich regions (dark color) possess smaller potential than the surrounding P3HT-rich regions (light color). When the standard sample of P3HT/TiO_2 nanorod film is illuminated with a white light source, the surface potential images show greater contrast, allowing much easier identification of TiO_2 nanorod-rich regions from the P3HT matrix (Figure 4b). Upon illumination, the excitons are separated at the interfaces, leading to the TiO_2 nanorod-rich regions becoming more negatively charged and the surrounding P3HT-rich regions becoming positively charged. The formation of P3HT phase is highly dependent on the device fabrication methods and materials. The brighter regions in the surface potential image are the P3HT-rich domain. The variation of shape and connectivity of the brighter region reveals differences in the formation of P3HT network.

Surface potential images were also measured for the film processed by low boiling CF as shown in Figure 4c in dark and Figure 4d under illumination. They reveal the bicontinuous structure of respective P3HT- and TiO_2 nanorod-rich phases on the film surface of the device. Connectivity within the P3HT-rich domains is reduced in this film due to a short film formation time from CF. For P3HT with molecular weight of 30K in the blend, the film shows less contrast between the donor material of P3HT-rich regions and acceptor material of TiO_2 nanorod-rich regions (Figure 4e in dark and Figure 4f under illumination), reflecting a less significant phase separation than the standard structure with 70K P3HT. The reduced extent of phase separation results in decreased domain size of charge transporting paths and increased interfacial area. This explains the reduced recombination resistance. Figure 4g,h reveal the surface potential images for the P3HT/dye-TiO_2 nanorod hybrid. The interconnectivity of the P3HT network is improved as compared to the standard sample, indicating the surface modification of TiO_2 nanorods facilitates growth of the P3HT network due to improved compatibility at the interfaces between hydrophobic P3HT and hydrophilic TiO_2.

Figure 5 summarizes the *I*−*V* curves of different devices under AM 1.5 G illumination. As compared with the standard device, a reduction in recombination resistance corresponds to lower fill factor and overall efficiency in device *I*−*V* response under illumination for device 2 with chloroform and device 3 with 30K P3HT. The P3HT/dye-TiO_2 nanorod device exhibits the largest recombination resistance among the samples and results in the best overall solar cell efficiency with I_{SC} of 2.70 mA/cm^2, V_{OC} of 0.80 V, FF of 0.57, and power conversion efficiency (PCE) of 1.24%, while the standard device exhibits I_{SC} of 1.59 mA/cm^2, V_{OC} of 0.67 V, FF of 0.44, and power conversion efficiency (PCE) of 0.47%. The PCE for the device made with dye-modified TiO_2 is increased to 2.6 times that of the device made with unmodified TiO_2.

At open circuit voltage of the solar cells, the electron lifetime among these devices is in the ascending order third device P3HT(30K, CB)/TiO_2 (19.1 μs) < second device P3HT(70K, CF)/TiO_2 (25.7 μs) < standard device P3HT(70K, CB)/TiO_2 (32.8 μs) < fourth device P3HT(70K, CB)/dye-TiO_2 (53.8 μs). The hybrid film roughness among these devices is in the descending order second device (17.8 nm) > third device (6.7 nm) > standard device (4.6 nm) > fourth device (3.8 nm). In addition, the obtained efficiency of solar cells is in the ascending order second device (0.33%) < third device (0.44%) < standard device (0.47%) < fourth device (1.24%). These results suggest the type of heterostructure and charge carrier lifetime is highly correlated with the solar cell performance.

By using the laser flash photolysis system and the femtosecond transient absorption system, the charge recombination rate and carrier lifetime of TiO_2 nanorod with different surface ligands has been studied.[37] It is reported that, by anchoring the surface ligand, oligo-3HT-COOH, onto TiO_2 nanorod, the charge carrier lifetime is increased from 42 μs to 12 ms. Here we report the similar trend that the anchoring of W-4 dye on TiO_2 nanorod can decrease the recombination rate and increase charge carrier lifetime in the hybrid P3HT/TiO_2 nanorod solar cell. The technique of impedance spectroscopy study provides a facile method to determine the recombination rate and charge carrier lifetime in a finished solar cell device.

CONCLUSIONS

The factors of P3HT/TiO_2 nanorod film morphology and interfacial properties that influence recombination in P3HT/TiO_2 nanorod solar cells are studied. The results of impedance spectroscopy investigation indicate the variation of charge recombination rate correlates with evaluation of the phase separation of respective donor and acceptor phases. The interfacial property is crucial for charge recombination in the device. Anchoring a layer of dye on TiO_2 nanorod greatly reduces the recombination rate. Finally, the device *I*−*V* characteristics under illumination are highly dependent on the recombination rate. The lowest recombination rate device exhibits the largest power conversion efficiency.

ASSOCIATED CONTENT

Supporting Information. Additional information as noted in the text. This material is available free of charge via the Internet at http://pubs.acs.org.

AUTHOR INFORMATION

Corresponding Author

*Telephone 886-2-33664078; fax 886-2-33664078; e-mail suwf@ntu.edu.tw.

■ ACKNOWLEDGMENT

We thank the National Science Council of Republic of China (99-2120-M-002-011; 98-3114-E-002-001) for financial support of this research.

■ REFERENCES

(1) Ma, W.; Yang, C; Gong, X; Lee, K.; Heeger, A. J. *Adv. Funct. Mater.* **2005**, *15*, 1617.
(2) Park, S.-H.; Roy, A.; Beaupré, S.; Cho, S.; Coates, N.; Moon, J.-S.; Moses, D.; Leclerc, M.; Lee, K.; Heeger, A. J. *Nat. Photonics* **2009**, *3*, 297.
(3) Chen, H.-Y.; Hou, J.; Zhang, S.; Liang, Y.; Yang, G.; Yang, Y.; Yu, L.; Wu, Y.; Li, G. *Nat. Photonics* **2009**, *3*, 649.
(4) Green, M. A.; Emery, K.; Hishikawa, Y.; Warta, W. *Prog. Photovoltaics* **2011**, *19*, 84.
(5) Shaheen, S. E.; Brabec, C. J.; Sariciftci, N. S.; Padinger, F.; Fromherz, T.; Hummelen, J. C. *Appl. Phys. Lett.* **2001**, *78*, 841.
(6) Yang, X. N.; Loos, J.; Veenstra, S. C.; Verhees, W. J. H.; Wienk, M. M.; Kroon, J. M.; Michels, M. A. J.; Janssen, R. A. J. *Nano Lett.* **2005**, *5*, 579.
(7) Greenham, N. C.; Peng, X.; Alivisatos, A. P. *Phys. Rev. B* **1996**, *54*, 17628.
(8) Huynh, W. U.; Dittmer, J. J.; Alivisatos, A. P. *Science* **2002**, *29*, 2425.
(9) Mora-Seró, I.; Bisquert, J.; Fabregat-Santiago, F.; Garcia-Belmonte, G.; Zoppi, G.; Durose, K.; Proskuryakov, Y.; Oja, I.; Belaidi, A.; Dittrich, T.; Tena-Zaera, R.; Katty, A.; Lévy-Clément, C.; Barrioz, V.; Irvine, S. J. C. *Nano Lett.* **2006**, *6*, 640.
(10) O'Hayre, R.; Nanu, M.; Schoonman, J.; Goossens, A.; Wang, Q.; Grätzel, M. *Adv. Funct. Mater.* **2006**, *16*, 1566.
(11) Mora-Seró, I.; Giménez, S.; Fabregat-Santiago, F.; Gómez, R.; Shen, Q.; Toyoda, T.; Bisquert, J. *Acc. Chem. Res.* **2009**, *42*, 1848.
(12) Barea, E. M.; Shalom, M.; Giménez, S.; Hod, I.; Mora-Seró, I.; Zaban, A; Bisquert, J. *J. Am. Chem. Soc.* **2010**, *132*, 6834.
(13) Garcia-Belmonte, G.; Munar, A.; Barea, E. M.; Bisquert, J.; Ugarte, I.; Pacios, R. *Org. Electron.* **2008**, *9*, 847.
(14) Garcia-Belmonte, G.; Boix, P. P.; Bisquert, J.; Sessolo, M.; Bolink, H. J. *Sol. Energy Mater. Sol. Cells* **2010**, *94*, 366.
(15) Kuwabara, T.; Kawahara, Y.; Yamaguchi, T.; Takahashi, K. *Appl. Mater. Interfaces* **2009**, *10*, 2107.
(16) Kuwabara, T.; Nakamoto, M.; Kawahara, Y.; Yamaguchi, T.; Takahashi, K. *J. Appl. Phys.* **2009**, *105*, No. 124513.
(17) Huang, W.; Peng, J.; Wang, L.; Wang, J.; Cao, Y. *Appl. Phys. Lett.* **2008**, *92*, No. 013308.
(18) Wang, M.; Grätzel, C.; Moon, S.-J.; Humphry-Baker, R.; Rossier-Iten, N.; Zakeeruddin, S. M.; Grätzel, M. *Adv. Funct. Mater.* **2009**, *19*, 2163.
(19) Barea, E. M.; Caballero, R.; Fabregat-Santiago, F.; De La Cruz, P.; Lango, F.; Bisquert, J. *ChemPhysChem* **2010**, *11*, 245.
(20) Campbell, I. H.; Smith, D. L.; Ferraris, J. P. *Appl. Phys. Lett.* **1995**, *22*, 3030.
(21) Lin, Y.- Y.; Chu, T.-H.; Li, S.-S.; Chuang, C.-H.; Chang, C.-H.; Su, W.-F.; Chang, C.-P.; Chu, M.-W.; Chen, C.-W. *J. Am. Chem. Soc.* **2009**, *131*, 3644.
(22) Beek, W. J. E.; Wienk, M. M.; Kemerink, M.; Yang, X.; Janssen, R. A. J. *J. Phys. Chem. B* **2005**, *109*, 9505.
(23) Kwong, C. Y.; Choy, W. C. H.; Djurisic, A. B.; Chui, P. C.; Cheng, K. W.; Chan, W. K. *Nanotechnology* **2004**, *15*, 1156.
(24) Yen, W.-C.; Lee, Y.-H.; Lin, J.-F.; Dai, C.-A.; Feng, U.-S.; Su, W.-F. *Langmuir* **2010**, *27*, 109.
(25) Holder, E.; Tessler, N.; Rogach, A. *J. Mater. Chem.* **2008**, *18*, 1064.
(26) Chang, J. F.; Sun, B.; Breiby, D. A.; Nielsen, M. M.; Sölling, T. I.; Giles, M.; McCulloch, I.; Sirringhaus, H. *Chem. Mater.* **2004**, *16*, 4772.
(27) Schilinsky, P.; Asawapirom, U.; Scherf, U.; Biele, M.; Brabec, C. J. *Chem. Mater.* **2005**, *17*, 2175.
(28) Zhao, K.; Xue, L.; Liu, J.; Gao, X.; Wu, S.; Han, Y.; Geng, Y. *Langmuir* **2010**, *26*, 471.
(29) Zhao, Y.; Shao, S.; Xie, Z.; Geng, Y.; Wang., L. *J. Phys. Chem. C* **2009**, *113*, 17235.
(30) Hoppe, H.; Glatzel, T.; Niggemann, M.; Hinsch, A.; Lux-Steiner, M. Ch.; Sariciftci, N. S. *Nano Lett.* **2005**, *5*, 269.
(31) Palermo, V.; Ridolfi, G.; Talarico, A. M.; Favaretto, L.; Barbarella, G.; Camaioni, N.; Samorí, P. *Adv. Funct. Mater.* **2007**, *17*, 472.
(32) Liscio, A.; Luca, G. D.; Nolde, F.; Palermo, V.; Müllen, K.; Samorì, P. *J. Am. Chem. Soc.* **2008**, *130*, 780.
(33) Zeng, T.-W.; Hsu, F.-C.; Tu, Y.-C.; Lin, T.-H.; Su, W.-F. *Chem. Phys. Lett.* **2009**, *479*, 105.
(34) Wu, M.-C.; Wu, Y.-J.; Yen, W.-C.; Lo, H.-H.; Lin, C.-F.; Su, W.-F. *Nanoscale* **2010**, *2*, 1448.
(35) Ravirajan, P.; Peiro, A. M.; Nazeeruddin, M. K.; Graetzel, M.; Bradley, D. D. C.; Durrant, J. R.; Nelson, J. *J. Phys. Chem. B* **2006**, *110*, 7635.
(36) Lin, Y.-Y.; Lee, Y.-Y.; Chang, L.; Wu, J.-J.; Chen, C.-W. *Appl. Phys. Lett.* **2009**, *94*, No. 063308.
(37) Huang, Y.-C.; Yen, W.-C.; Liao, Y.-C.; Yu, Y.-C.; Hsu, C.-C.; Ho, M.-L.; Chou, P.-T.; Su, W.-F. *Appl. Phys. Lett.* **2010**, *96*, No. 123501.
(38) Mor, G. K.; Kim, S.; Paulose, M.; Varghese, O. K.; Shankar, K.; Basham, J.; Grimes, C. A. *Nano Lett.* **2009**, *9*, 4250.
(39) Chuangchote, S.; Sagawa, T.; Yoshikawa, S. *J. Mater. Res.* **2011**, *26*, 2316.
(40) Cozzoli, P. D.; Kornowski, A.; Weller, H. *J. Am. Chem. Soc.* **2003**, *125*, 14539.
(41) Zeng, T.-W.; Lin, Y.-Y.; Chen, C.-W.; Chen, C.-H.; Liou, S.-C.; Huang, H.-Y.; Su, W.-F. *Nanotechnology* **2006**, *17*, 5387.
(42) Loewe, R, S.; Khersonsky, S. M.; McCullough, R. D. *Adv. Mater.* **1999**, *11*, 250.
(43) Liu, Y.; Scully, S. R.; McGehee, M. D.; Liu, J.; Luscombe, C. K.; Fréchet, J. M. J.; Shaheen, S. E.; Ginley, D. S. *J. Phys. Chem. B* **2006**, *110*, 3257.